




**ORIGINAL ARTICLE**

# N471D WASH complex subunit strumpellin knock-in mice display mild motor and cardiac abnormalities and BPTF and KLHL11 dysregulation in brain tissue

Christoph S. Clemen<sup>1,2,3</sup>  | Andreas Schmidt<sup>4</sup> | Lilli Winter<sup>5,6</sup>  |  
 Fabio Canneva<sup>7</sup> | Ilka Wittig<sup>8</sup> | Lore Becker<sup>9</sup> | Roland Coras<sup>5</sup> |  
 Carolin Berwanger<sup>1</sup> | The German Mouse Clinic Consortium | Andreas Hofmann<sup>10</sup> |  
 Britta Eggers<sup>11</sup> | Katrin Marcus<sup>11</sup> | Valerie Gailus-Durner<sup>9</sup> | Helmut Fuchs<sup>9</sup> |  
 Martin Hrabe de Angelis<sup>9,12,13</sup> | Marcus Krüger<sup>4</sup> | Stephan von Hörsten<sup>7</sup> |  
 Ludwig Eichinger<sup>3</sup> | Rolf Schröder<sup>5</sup> 

<sup>1</sup>Institute of Aerospace Medicine, German Aerospace Center, Cologne, Germany

<sup>2</sup>Center for Physiology and Pathophysiology, Institute of Vegetative Physiology, Medical Faculty, University of Cologne, Cologne, Germany

<sup>3</sup>Center for Biochemistry, Institute of Biochemistry I, Medical Faculty, University of Cologne, Cologne, Germany

<sup>4</sup>Center for Molecular Medicine and Excellence Cluster "Cellular Stress Responses in Aging-Associated Diseases" (CECAD), University of Cologne, Cologne, Germany

<sup>5</sup>Institute of Neuropathology, University Hospital Erlangen, Friedrich-Alexander University Erlangen-Nürnberg, Erlangen, Germany

<sup>6</sup>Neuromuscular Research Department, Center for Anatomy and Cell Biology, Medical University of Vienna, Vienna, Austria

<sup>7</sup>Experimental Therapy, University Hospital Erlangen and Preclinical Experimental Center, Friedrich-Alexander University Erlangen-Nürnberg, Erlangen, Germany

<sup>8</sup>Functional Proteomics, Medical School, Goethe University, Frankfurt, Germany

<sup>9</sup>Institute of Experimental Genetics, German Mouse Clinic, Helmholtz Zentrum München, German Research Center for Environmental Health, Neuherberg, Germany

<sup>10</sup>Faculty of Veterinary and Agricultural Sciences, University of Melbourne, Parkville, Victoria, Australia

<sup>11</sup>Medical Proteome Center, Medical Faculty, and Medical Proteome Analysis, Center for Protein Diagnostics (PRODI), Ruhr-University Bochum, Bochum, Germany

<sup>12</sup>TUM School of Life Sciences (SoLS), Technical University of Munich, Freising, Germany

<sup>13</sup>German Center for Diabetes Research (DZD), Neuherberg, Germany

**Correspondence**

Christoph S. Clemen, Institute of Aerospace Medicine, German Aerospace Center (DLR), Linder Höhe, 51147 Cologne, Germany.  
Email: christoph.clemen@dlr.de

Rolf Schröder, Institute of Neuropathology, University Hospital Erlangen, Schwabachanlage 6, 91054 Erlangen, Germany.  
Email: rolf.schroeder@uk-erlangen.de

**Funding information**

Deutsche Forschungsgemeinschaft, Grant/Award Number: FOR5046/P5;

**Abstract**

**Aims:** We investigated N471D WASH complex subunit strumpellin (*Washc5*) knock-in and *Washc5* knock-out mice as models for hereditary spastic paraplegia type 8 (SPG8).

**Methods:** We generated heterozygous and homozygous N471D *Washc5* knock-in mice and subjected them to a comprehensive clinical, morphological and laboratory parameter screen, and gait analyses. Brain tissue was used for proteomic analysis. Furthermore, we generated heterozygous *Washc5* knock-out mice. WASH complex subunit strumpellin expression was determined by qPCR and immunoblotting.

**Results:** Homozygous N471D *Washc5* knock-in mice showed mild dilated cardiomyopathy, decreased acoustic startle reactivity, thinner eye lenses, increased alkaline

A full list of consortium members and their affiliations is provided in the Appendix A.

[Correction added on OCT 5 2021, after first online publication: Peer review history statement has been added.]

This is an open access article under the terms of the Creative Commons Attribution-NonCommercial-NoDerivs License, which permits use and distribution in any medium, provided the original work is properly cited, the use is non-commercial and no modifications or adaptations are made.

© 2021 The Authors. *Neuropathology and Applied Neurobiology* published by John Wiley & Sons Ltd on behalf of British Neuropathological Society.

German Federal Ministry of Education and Research, Grant/Award Number: 01KX1012; German Center for Diabetes Research; Cardio Pulmonary Institute, Grant/Award Number: EXC2026

phosphatase and potassium levels and increased white blood cell counts. Gait analyses revealed multiple aberrations indicative of locomotor instability. Similarly, the clinical chemistry, haematology and gait parameters of heterozygous mice also deviated from the values expected for healthy animals, albeit to a lesser extent. Proteomic analysis of brain tissue depicted consistent upregulation of BPTF and downregulation of KLHL11 in heterozygous and homozygous knock-in mice. WASHC5-related protein interaction partners and complexes showed no change in abundancies. Heterozygous *Washc5* knock-out mice showing normal WASHC5 levels could not be bred to homozygosity.

**Conclusions:** While biallelic ablation of *Washc5* was prenatally lethal, expression of N471D mutated WASHC5 led to several mild clinical and laboratory parameter abnormalities, but not to a typical SPG8 phenotype. The consistent upregulation of BPTF and downregulation of KLHL11 suggest mechanistic links between the expression of N471D mutated WASHC5 and the roles of both proteins in neurodegeneration and protein quality control, respectively.

#### KEYWORDS

N471D strumpellin knock-in mice, BPTF, HSP (hereditary spastic paraplegia), KLHL11, NURF, SPG8, strumpellin, WASH complex subunit 5

## INTRODUCTION

Mutations of the human WASH complex subunit strumpellin gene (synonyms: WASH complex subunit 5 gene, *WASHC5*, *KIAA0196*, *SPG8*, *RTSC1*) on chromosome 8q24.13 cause autosomal-dominant spastic paraplegia 8 (SPG8, OMIM #603563) [1, 2] and autosomal-recessive Ritscher-Schinzel syndrome 1 (RTSC1, OMIM #220210) [3, 4]. SPG8 is a subform of the clinically and genetically highly diverse group of hereditary spastic paraplegias that are clinically characterised by a slowly progressive weakness and spasticity of the lower limbs [5–7]. Ritscher-Schinzel syndrome is a developmental multi-organ disease with craniofacial, cerebellar and cardiac abnormalities [4, 8]. To date, 18 different SPG8-causing mutations have been reported comprising 16 missense mutations, a single frameshift mutation, and one multi-exonic deletion mutation [1, 2, 9–15]; the genetic basis of Ritscher-Schinzel syndrome 1 is a homozygous splice site mutation [3, 4]. An autopsy of a 70-year-old female SPG8 patient harbouring the heterozygous p.V626F mutation revealed a severe atrophy of the thoracic spinal cord in conjunction with demyelination and loss of neurons in this region [16].

Human *WASHC5* encodes WASH complex subunit 5 (WASHC5), an evolutionarily conserved protein of 1159 amino acids with a calculated molecular mass of 134 kDa. Although no three-dimensional structural information for this protein is currently available, in silico analysis of the overall domain organisation revealed a topology consisting of an N-terminal part followed by a central domain composed of five spectrin-like repeats, and a C-terminal part [17, 18] (Figure 1A). The pathophysiology of both *WASHC5*-related diseases is an unresolved issue. A previous study addressed the consequences of the targeted ablation of *Washc5* in mice [13]. Whereas homozygous *Washc5* knock-out mice showed embryonic lethality, heterozygous animals were reported to display reduced WASHC5 levels, but no clinical abnormalities. In particular, no gait abnormalities indicative of a hereditary spastic

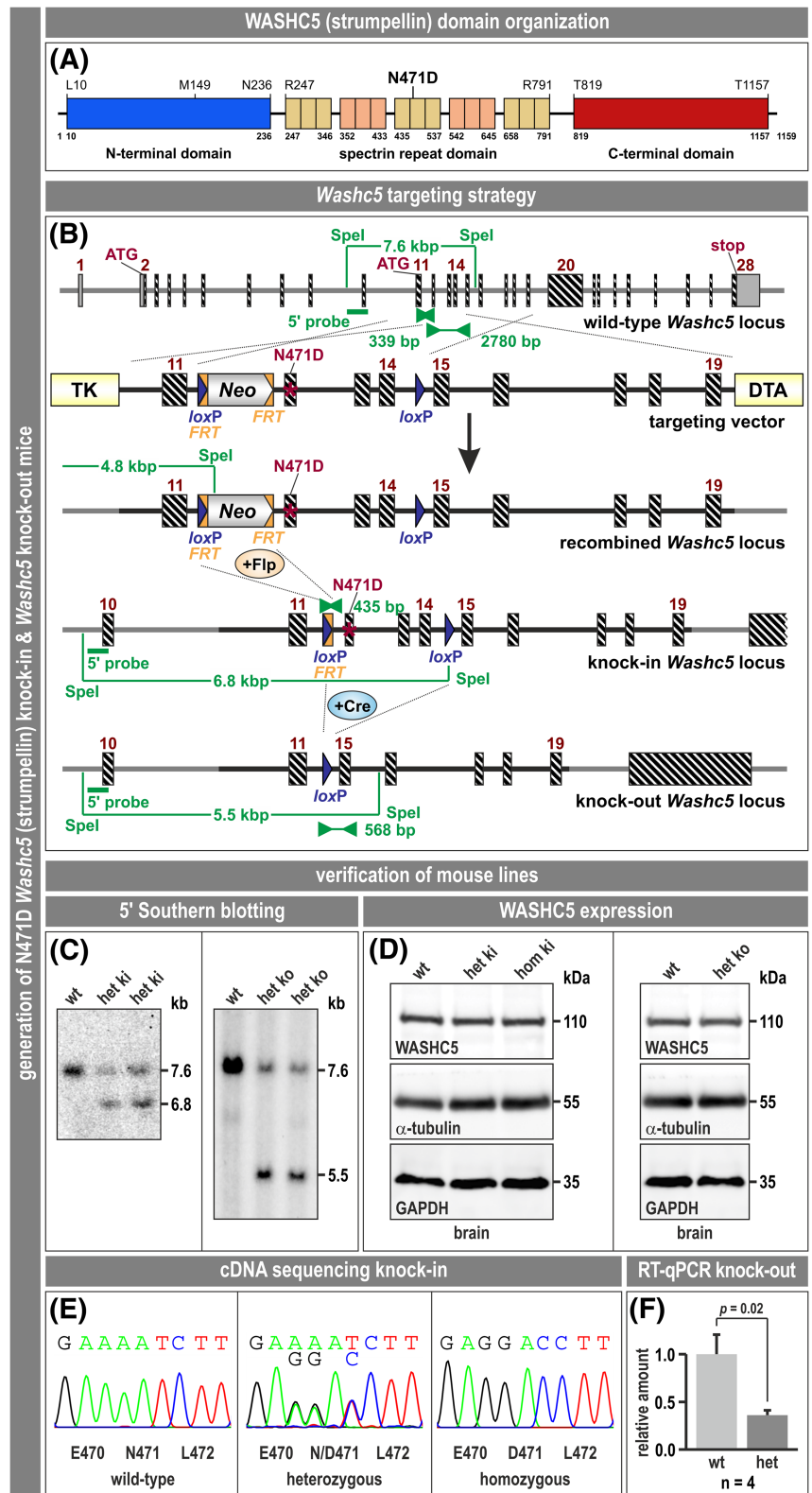
#### Key points

- *WASHC5* mutations cause hereditary spastic paraplegia type 8 and Ritscher-Schinzel syndrome 1.
- N471D *Washc5* knock-in mice showed mild dilated cardiomyopathy, gait abnormalities, and other clinical and laboratory parameter deviations.
- N471D *Washc5* knock-in mice did not show a typical hereditary spastic paraplegia type 8 phenotype.
- Biallelic ablation of *Washc5* in mice was prenatally lethal.
- N471D *Washc5* knock-in mice displayed consistent upregulation of BPTF and downregulation of KLHL11 in brain tissue.

paraplegia phenotype were described for the heterozygous animals. Thus, the monoallelic inactivation of *WASHC5* appeared not to be sufficient to induce a hereditary spastic paraplegia phenotype.

In the present study, we report the generation and characterisation of hetero- and homozygous WASH complex subunit strumpellin knock-in mice harbouring the p.N471D (c.1411\_1413delA-AT>insGAC) missense mutation, which causes human SPG8 [1]. This knock-in mouse line represents a valid genetic in vivo model for autosomal-dominant SPG8, as the expression of the point-mutated WASHC5 is controlled by the endogenous gene regulation sites. In addition, we generated WASH complex subunit strumpellin knock-out mice, which, however, showed normal WASHC5 levels in the heterozygous state and could not be bred to homozygosity. Notably, in heterozygous and homozygous N471D WASH complex subunit strumpellin knock-in mice, our comprehensive phenotypic screen revealed multiple, yet mild gait, cardiac, eye and blood changes.

**FIGURE 1** WASHC5 domain scheme, *Washc5* targeting strategy, and mouse line verification. (A) Schematic domain structure of WASHC5. The protein consists of a central spectrin repeat domain flanked by N- and C-terminal domains. Amino acid positions of domain borders and spectrin repeats are indicated. The SPG8 causing missense mutation N471D resides in the third spectrin repeat. (B) Scheme of the genomic targeting strategy resulting in N471D *Washc5* knock-in as well as *Washc5* knock-out mouse lines. In a classical, recombination-based gene targeting approach, the codon ‘AAT’ encoding asparagine (N) was replaced by ‘GAC’ encoding aspartic acid (D) in exon 12 followed by Flp-mediated removal of the neomycin selection cassette thus leading to the generation of N471D *Washc5* knock-in mice. Note that the chosen strategy also allowed the inactivation of the WASH complex subunit 5 gene via Cre-mediated deletion of exons 12 to 14 leading to the generation of *Washc5* knock-out mice. (C) Both mouse lines were verified by southern blotting. (D) WASHC5 immunoblotting revealed no obvious changes in the signal intensities in brain tissue derived from heterozygous and homozygous knock-in mice and heterozygous knock-out mice as compared with the respective wild-type littermates. (E) In *Washc5* knock-in mice the expression of the mutated mRNA coding for D471 WASHC5 was confirmed by RT-PCR in conjunction with sequencing of the PCR products. Note that the wild-type sequence GAA AAT CTT was mutated into GAG GAC CTT with the silent mutation of codon E470 to generate an EcoO109I restriction site in addition to the N471D missense mutation. (F) Reverse transcription quantitative real-time polymerase chain reaction (RT-qPCR) depicted a significant reduction of WASH complex subunit 5 mRNA levels in brain tissue derived from heterozygous *Washc5* knock-out mice as compared with wild-type littermates



Moreover, using deep proteomic analysis we determined a consistent upregulation of BPTF and downregulation of KLHL11 in brain tissue of both hetero- and homozygous knock-in mice.

## MATERIALS AND METHODS

### Animals

Heterozygous and homozygous N471D (p.Asn471Asp, c.1411\_1413delAAT>insGAC) WASH complex subunit strumpellin knock-in mice B6J.129SvPas-*Washc5*<sup>tm1.1Ccrs</sup> (<http://www.informatics.jax.org/allele/MGI:6246601>) and their wild-type siblings as well as heterozygous WASH complex subunit strumpellin knock-out mice B6J.129SvPas-*Washc5*<sup>tm1.2Ccrs</sup> (<http://www.informatics.jax.org/allele/MGI:6507388>) and their wild-type siblings were used. Both mouse lines were generated according to our specifications (CSC, RS) by genOway, Lyon, France (Figure 1B). Routine polymerase chain reaction (PCR) genotyping of N471D *Washc5* knock-in mice was performed using primer pair 75525flp 5'-ACTCTCTGCTGTACCTCACAGTTCTGACG-3' and 75526flp 5'-CCACAATACTCCAGCCATCAACAGC-3' resulting in products of 339 bp for the wild-type and 435 bp for the knock-in alleles, and of *Washc5* knock-out mice using primer pair 75509cre 5'-CCCAGAACCCAAATCTTTATCCACC-3' and 75510cre 5'-TTAAGGAAGCAGCTATCAGAGGCAGTCC-3' amplifying 2780 bp and 568 bp products for the wild-type and knock-out alleles, respectively. Mice were housed in isolated ventilated cages (IVCs) under specific and opportunistic pathogen-free (SOPF) conditions in a standard environment with free access to water and food. Health monitoring was done as recommended by the Federation of European Laboratory Animal Science Associations (FELASA). Mice were handled in accordance with the German Animal Welfare Act (*Tierschutzgesetz*) as well as the German Regulation for the protection of animals used for experimental or other scientific purposes (*Tierschutz-Versuchstierverordnung*). All investigations were approved by the governmental office for animal care (*Landesamt für Natur, Umwelt und Verbraucherschutz North Rhine-Westphalia* [LANUV NRW], Recklinghausen, Germany [reference numbers 8.87-50.10.47.09.014 and 84-02.05.40.14.057]). At the German Mouse Clinic (GMC), mice were maintained in IVCs with water and standard mouse chow according to the directive 2010/63/EU, German laws, and GMC housing conditions. All tests were approved by the responsible authority of the district government of Upper Bavaria, Germany.

The targeting vector for the development of the N471D WASH complex subunit strumpellin knock-in mice with subsequent access to the WASH complex subunit strumpellin knock-out mice (Figure 1B) was constructed from 129Sv/Pas mouse line genomic DNA. The missense mutation coding for D471 was inserted into exon 12 in conjunction with insertion of a neomycin selection cassette flanked by FRT sites in intron 12 as well as floxing of exons 12 to 14 including the point mutation. 5' to the 3.4 kb short homology arm the targeting vector contained a thymidine kinase (TK) negative selection cassette; the length of the 3' long homology arm was 6.8 kb followed at its 3' end by a diphtheria toxin A (DTA) negative selection cassette to

enhance the chance of isolating ES cell clones harbouring the distal loxP site. Linearized targeting vector was transfected into 129Sv ES cells (genOway, Lyon, France; electroporation of 10<sup>8</sup> ES cells in presence of 100 µg of linearized plasmid at 260 V and 500 µF). Positive selection was started 48 h after electroporation by addition of 200 µg/ml of G418 (150 µg/ml of active component, Life Technologies, Inc.). A total number of 1374 G418-resistant ES cell clones were isolated, amplified in 96-well plates, and duplicates of the ES cell clones grown on gelatine were genotyped by both PCR and Southern blot analysis. For PCR analysis, a primer pair was used to amplify the 5' targeted region, external primer 75489sa, 5'-TCTCTGACTCAAGCAACAGATTTTTCCG-3', and neomycin cassette primer 0067-Neo-13172sa, 5'-GAACTTCTGACTAGGGGAGGAGTAGAAGG-3'. A second primer pair, 0070-Neo-16219sa, 5'-CCTGCTCTTTACTGAAGGC TCTTTACTATTGC-3', and 75491seq-RSC3a, 5'-ACATATCTGTTTCTTGCTTCATAAATGCCCTAG-3', was used to amplify the 3' targeted region and to verify the N471D point mutation integration by sequencing of the PCR product. The correct targeting event was further verified by Southern blot analysis using internal (neomycin cassette) as well as external probes on both the 5' and 3' sites. Finally, only a single ES cell clone (#190-G2) was identified as fully correctly targeted at the *Washc5* locus also including the 3' distal loxP site. ES cells from this clone were microinjected into C57BL/6J blastocysts and gave rise to few male chimeras with a significant ES cell contribution as determined by an agouti coat colour which were crossbred with C57BL/6 mice expressing Flp recombinase to remove the neomycin selection cassette from intron 11. Resulting N471D *Washc5* knock-in mice were identified using genotyping primer pair 75525flp and 75526flp as given above. Further, the male chimeras were crossbred with C57BL/6 mice expressing Cre recombinase to remove the point mutated exon 12 and exons 13 to 14 for generation of the constitutive *Washc5* knock-out mice; identification of the knock-out mice was done with the above-mentioned primer pair 75509cre and 75510cre. Moreover, the founder N471D *Washc5* knock-in and *Washc5* knock-out animals were validated by Southern blotting using a 5' external probe.

### Phenotypic analysis at the GMC

N471D *Washc5* knock-in mice and wild-type control littermates were subjected to a systematic, comprehensive phenotyping at the GMC at the *Helmholtz Zentrum München* (<http://www.mouseclinic.de>) as described previously [19–21]. This phenotyping covers a broad range of parameters in the areas of immune regulation, behaviour, cardiovascular function, clinical chemistry, dysmorphology, energy metabolism, eye analysis and vision, haematology, immunology, neurology and pathology. In particular, the latter also included the neuropathological analysis of brain, spinal cord and sciatic nerve tissue specimens. The phenotypic tests were performed according to standardised protocols as described before [22]. Any variations of these protocols and additional tests are specified in this current study. Depending on the test performed, the animal number varied and is indicated in the phenotyping report (accessible at <http://tools.mouseclinic.de/>

phenomap/phenomap.html under the project name 'Strumpellin\_KI'. Data were analysed using R (Version 3.2.3); tests for genotype effects were made by using Student's *t* test, Wilcoxon rank sum test, linear models, or ANOVA and post hoc tests, or Fisher's exact test depending on the assumed distribution of the parameter and the questions addressed to the data. A *p* value  $\leq 0.05$  was used as threshold of significance. The GMC data set was not corrected for multiple testing. The genotype of all mice used for analysis was verified by PCR analysis.

## Gait analyses

The DigiGait system (Mouse Specifics, Boston, USA) allows mice to walk on a motorised transparent treadmill belt, below which a video camera is mounted to capture the image of the animals' ventral side. The DigiGait software generates 'digital paw prints' and dynamic gait signals, thus accumulating a temporal record of paw placement relative to the treadmill belt. The acquired data afford automatic identification of the portions of the paws that are and are not in contact with the treadmill belt. A total of 37 gait parameters were calculated from at least 11 strides for different walking speeds. Data analysis was performed as described above.

A further, quantitative assessment of gait and locomotion was performed using the CatWalk XT system (Noldus Information Technology, Wageningen, the Netherlands). In general, the system is composed of an enclosed alley on a glass plate with mice being able to walk through voluntarily. The glass plate is illuminated with green light under conditions of total internal reflection. At each contact of a paw with the glass plate, light is refracted at the opposite site and captured by a video-camera below the alley. For each mouse, 20 voluntary runs, without use of any attractants, were recorded in rounds of five runs each, with a maximum of 10 runs per day to reduce habituation. All acquisitions were recorded in the dark, with minimal external disruption. Investigation of all runs was performed using the Illuminated Footprint technology and the CatWalk 10.6 software. The light intensity threshold of the refracted light was set to 0.12 and a camera gain of 23.22 dB was used. Additionally, all runs were also evaluated manually, in order to exclude those runs, showing unwanted behaviours like sniffing, exploring or sitting. Toe spread and print length for all completely detected footprints were measured interactively using the software. All procedures, including silhouette-length dependent parameter-scaling, for example, stride length and correction for transgene-dependent differences as well as subsequent systematic data analysis and data mining by heat mapping, were performed as recently described [23, 24] and refined [25, 26]. The ontology of the resulting parameters was functionally clustered into three different groups, (i) static, single paw parameters; (ii) dynamic, time-dependent parameters; and (iii) interdependent parameters. Finally, a representative parameter of each group (hind stride length, hind base of support and hind swing speed) was analysed in detail, based on the mean value of all investigated runs for an individual across repeated measurements. The genotype of all mice used for analysis was verified by PCR analysis.

## Antibodies and immunoblotting

For sodium dodecyl sulphate-polyacrylamide gel electrophoresis (SDS-PAGE) and immunoblotting, liquid nitrogen snap-frozen tissue samples were ground in a mortar at  $-80^{\circ}\text{C}$  and solubilised in a buffer containing 10% SDS as described in Winter et al. [27]. Primary antibodies for immunoblotting were WASHC5 (strumpellin), rabbit polyclonal, 1:500, sc-87442, SantaCruz; GAPDH, rabbit polyclonal, 1:10,000, G9545, Sigma-Aldrich; and  $\alpha$ -tubulin, mouse monoclonal, 1:4000, T6074, Sigma-Aldrich; all diluted in phosphate-buffered saline with Tween 20 detergent (PBS-T) with 5% milk powder.

## Proteomic analysis of brain tissue

Brain hemispheres from 23 male mice at 25 month of age, 8  $\times$  heterozygous and 7  $\times$  homozygous N471D *Wasc5* knock-in mice and 8  $\times$  wild-type siblings, were dissected and liquid nitrogen snap-frozen; the genotype of all mice used for tissue preparation was verified by PCR analysis. Frozen brain samples were homogenised with an Ultra Turrax device (IKA) in extraction buffer (10% SDS, 150-mM NaCl, 50-mM HEPES, pH 7.8; 1-ml buffer per 100-mg tissue). Preclearing of samples was done by 10 min centrifugation at  $10,000 \times g$ . Supernatants were subjected to a Lowry protein quantitation assay [28] by using the DC Protein Assay (BioRad, #500-0116). From each sample, 150  $\mu\text{g}$  of protein were diluted in 4% (w/v) SDS, 100-mM HEPES, pH 7.6, 150-mM NaCl, 0.1-M DTT, mixed with 200- $\mu\text{l}$  8-M Urea, 50-mM Tris/HCl, pH 8.5, and loaded onto spin filters with a 30-kDa cut-off (Microcon) according to the filter-aided sample preparation protocol [29]. Proteins were digested overnight with trypsin/LysC (sequencing grade, Promega). Peptides were loaded on multi-stop-and-go tip (StageTip) containing C18 discs followed by fractionation on strong cationic exchange chromatography (SCX)-StageTips [30]. All fractions of each sample were eluted in wells of microtitre plates. Peptides were dried and resolved in 1% acetonitrile, 0.1% formic acid.

Liquid chromatography/mass spectrometry (LC/MS) was performed on a Thermo Scientific Q Exactive Plus spectrometer equipped with an ultra-high performance liquid chromatography unit (Thermo Scientific Easy-nLC) and a Nanospray Flex Ion-Source (Thermo Scientific). Peptides were separated using an in-house packed 2.4- $\mu\text{m}$  Reprosil C18 resin (Dr Maisch GmbH) picotip emitter tip (diameter 100  $\mu\text{m}$ , 15 cm long, New Objectives) eluted with a gradient from Eluent A (4% acetonitrile, 0.1% formic acid) to 30% Eluent B (80% acetonitrile, 0.1% formic acid) for 60 min followed by a second gradient to 60% B for 30 min. MS data were recorded by data-dependent acquisition using the Top10 method to select the most abundant precursor ions in positive mode for HCD fragmentation. The full MS scan range was 350 to 2000 *m/z* with a resolution of 70,000, and an automatic gain control (AGC) value of  $3 \times 10^6$  total ion counts with a maximal ion injection time of 80 ms. Only multi-valent ions (2+) were selected for MS/MS scans with a resolution of 17,500, an isolation window of 1.6 *m/z* and an AGC value set to  $10^5$  ions with a maximal ion injection time of 80 ms. Fullscan data were acquired in profile and fragments in centroid mode by Xcalibur software.

The obtained proteomics data were searched against a mouse protein sequence database (UniProtKB, TrEMBL, 05/2018) using the Andromeda search engine within the MaxQuant software (v. 1.6.1.0), whereby SCX fractions were defined as fractions of the respective sample. For cysteine, a fixed modification by carbamidomethylation was set; variable modifications were methionine S-oxidation and protein N-terminal acetylation. All false discovery rates (FDRs) were set to 0.01 to filter for most confident protein identifications. For protein quantitation, the label-free quantitation (LFQ) algorithm within MaxQuant was enabled and subsequently all protein LFQ values were  $\log_2$  transformed. All samples were z-score normalised and proteins with less than three LFQ values in all conditions were excluded from statistical analysis. Data obtained from heterozygous and homozygous N471D *Washc5* knock-in mice were individually compared with the wild-type sibling-derived data using a two-samples Student's *t* test in the Perseus software (v. 1.6.10.50); *p* values were corrected by the inbuilt permutation-based FDR calculation. Graphs were generated in Instant Clue [31].

## RESULTS

### N471D *Washc5* knock-in mice: A genetic model for human SPG8

In order to generate an N471D *Washc5* knock-in mouse line, we employed a classical, recombination-based gene targeting strategy to afford replacement of the codon “AAT” (in human “AAC”) encoding asparagine (N) by “GAC” (in human also “GAC”, [1]) encoding aspartic acid (D) in exon 12. Crossbreeding of the resulting mouse line with Flp deleter mice was used to remove the neomycin selection cassette (Figure 1B). Southern blotting (Figure 1C) and PCR genotyping confirmed the correct targeting event in the newly generated mouse line B6J.129SvPas-*Washc5*<sup>tm1.1Ccrs</sup> (<http://www.informatics.jax.org/allele/MGI:6246601>). The presence of the mutated mRNA species coding for D471 WASHC5 was confirmed by RT-PCR in conjunction with sequencing of the PCR products (Figure 1E). Note that the wild-type sequence GAA AAT CTT was mutated into GAG GAC CTT with the silent mutation of E470 to generate an EcoO109I restriction site in addition to the N471D missense mutation. Mating of heterozygous knock-in animals yielded offspring in a normal Mendelian distribution. Subsequently, we performed WASHC5 immunoblotting of total protein extracts from brain tissue, which showed no obvious changes in the signal intensities of the WASHC5 band in heterozygous and homozygous mice as compared with wild-type littermates (Figure 1D).

### Heterozygous *Washc5* knock-out mice show normal WASHC5 amounts, while homozygous ablation of *Washc5* is prenatally lethal

Our chosen targeting strategy with the two inserted loxP sites flanking exons 12 to 14 also allowed the inactivation of *Washc5* via crossbreeding with Cre deleter mice resulting in a constitutive *Washc5* knock-out

mouse line (Figure 1B). Southern blotting (Figure 1C) and PCR genotyping confirmed the correct targeting event in this second newly generated mouse line B6J.129SvPas-*Washc5*<sup>tm1.2Ccrs</sup> (<http://www.informatics.jax.org/allele/MGI:6507388>). Mating of heterozygous knock-out animals consistently failed to generate homozygous offspring, thus demonstrating that the homozygous ablation of *Washc5* is lethal in the prenatal development of mice. Quantitative real-time PCR demonstrated a reduction of WASH complex subunit strumpellin mRNA levels to 36% in brain tissue derived from heterozygous mice as compared with wild-type littermates (Figure 1F). However, WASHC5 immunoblotting showed identical signal intensities of the detected bands in heterozygous and wild-type animals (Figure 1D). This finding strongly argues against the presence of a haploinsufficiency-related phenotype, and we therefore decided to confine the comprehensive analysis to the N471D *Washc5* knock-in mouse line.

### Comprehensive phenotyping of N471D *Washc5* knock-in mice

Heterozygous and homozygous N471D *Washc5* knock-in mice and their wild-type siblings underwent a comprehensive screen at the GMC, Munich, addressing a broad range of parameters related to behaviour, neurology, cardiovascular system, ophthalmology, clinical chemistry, haematology, allergy, immunology, energy metabolism, general and bone-specific morphology as well as organ and tissue pathology. For this purpose, a number of 15 female and 15 male homozygous, 15 female and 17 male heterozygous mice and 15 female and 13 male wild-type siblings were subjected to the phenotypic analyses at the age of 11 months. An overview of the tests and a summary of the statistically significant, genotype-specific differences between homozygous (hom) knock-in (ki) animals and wild-type (wt) littermates are shown in Figure 2. For further detailed information with the full sets of data also including the results derived from heterozygous mice as well as sex-specific effects, please refer to the GMC database (accessible at <http://tools.mouseclinic.de/phenomap/phenomap.html> under the project name ‘Strumpellin\_KI’).

Our analyses disclosed a broad range of statistically significant alterations in homozygous mice in comparison with age- and sex-matched wild-type siblings. In transthoracic echocardiography, enlarged left ventricular chambers—assessed by left ventricular inner diameter during systole and diastole—with slightly increased left ventricular mass were observed in awake homozygous mice compared with wild-type controls. Stroke volume, an indicator of contraction of the myocardium compressing the ventricles, however, was slightly increased in the mutant animals compared with wild-type mice (Figure 2). While behavioural analyses addressing spontaneous reactions to a novel environment in the open field test showed no obvious genotype-specific effects, the acoustic startle reactivity at 110 dB was decreased in the homozygous animals, however, without any clear effect on prepulse inhibition. Laser interference biometry revealed thinner eye lenses in male homozygous mice in the ophthalmological analyses. Images of the retinal layering and of the fundus of

**FIGURE 2** Comprehensive phenotypic analysis of homozygous N471D *Washc5* knock-in mice. The analyses were conducted at the German Mouse Clinic, Munich, using a standardised workflow, which is summarised in this simplified overview. Values that are increased or decreased as compared with the wild-type littermate controls are highlighted in green or orange, respectively. Significant findings related to gait analyses are given in (Figure 3). Statistical significance was calculated by Student's *t* test, Wilcoxon rank sum test, linear models or ANOVA and post hoc tests, or Fisher's exact test as appropriate

screen	method/parameter	phenotype (hom N471D <i>Washc5</i> KI vs. WT)
allergy	IgE-ELISA	no significant/marked difference
	body surface temperature	no significant/marked difference
	transepidermal water loss	no significant/marked difference
behaviour	open field	no significant/marked difference
	acoustic startle amplitude (at 110 dB)	187.40 vs. 244.84 arb. unit, <i>p</i> =0.025
	prepulse inhibition	no significant/marked difference
cardiovascular system	electrocardiogram	no significant/marked difference
	left ventricular end-systolic internal diameter	1.71 vs. 1.35 mm, <i>p</i> =0.012
	left ventricular end-diastolic internal diameter	2.75 vs. 2.41 mm, <i>p</i> =0.003
	corrected left ventricular mass	25.92 vs. 22.78 mg, <i>p</i> =0.008
	stroke volume	20.56 vs. 13.75 $\mu$ L, <i>p</i> =0.01
	other parameters from echocardiography	no significant/marked difference
clinical chemistry	alkaline phosphatase	113.5 vs. 94.5 U/L, <i>p</i> =0.005
	potassium	4.53 vs. 4.33 mmol/L, <i>p</i> =0.032
	plasma lactate	9.12 vs. 9.83 mmol/L, <i>p</i> =0.045
	other parameters from autoanalyser	no significant/marked difference
	glucose tolerance test	no significant/marked difference
dysmorphology	visual inspection	no significant/marked difference
	X-ray	no significant/marked difference
	dual-energy X-ray absorptiometry	not analysed
energy metabolism	indirect calorimetry	no significant/marked difference
	qNMR	no significant/marked difference
ophthalmology	Scheimpflug imaging	no significant/marked difference
	optical coherence tomography	no significant/marked difference
	mean lens thickness	2.339 vs. 2.374 mm, <i>p</i> =0.0011 (only in male mice)
	other param. from laser interference biometry	no significant/marked difference
	virtual drum	no significant/marked difference
haematology	white blood cell counts	12.06 vs. 7.86 $10^3/\text{mm}^3$ , <i>p</i> <0.001
	haemoglobin	16.59 vs. 15.23 g/dL, <i>p</i> =0.045
	other blood counts	no significant/marked difference
immunology	flow cytometry	not analysed
	multiplex bead array	no significant/marked difference
neurology	hind paw clenching	significant effect, see figure 3
	other parameters from modified SHIRPA	no significant/marked difference
	2-paw and 4-paw grip strength	no significant/marked difference
	rotarod	no significant/marked difference
	beam ladder	no significant/marked difference
	balance beam	no significant/marked difference
	gait analysis (DigiGait & CatWalk analyses)	significant effects, see figure 3
	auditory brain stem response	no significant/marked difference
	nociception/hot plate	no significant/marked difference
pathology	macroscopy	no significant/marked difference
	standard histology (all organs/tissues)	no significant/marked difference
	PNS: sciatic nerve; CNS: brain, spinal chord	no significant/marked difference

the eye did not reveal any evident changes. In additional visual function testing, the homozygous mice had similar visual acuity as wild-type controls. Statistically significant findings in the clinical chemistry and haematology analyses were a rather mildly increased alkaline phosphatase level (to a lesser extent also present in heterozygous

mice), slightly increased potassium and lowered lactate levels and markedly increased white blood cell counts mainly in male homozygous and heterozygous mice as well as slightly elevated haemoglobin concentrations in homozygous animals (Figure 2). Mutant mice displayed neither morphological abnormalities nor radiological bone

pathology. All tests related to allergy and immunology, as well as energy metabolism showed values for the mutant mice that were in the range of the wild-type siblings. Moreover, a detailed macroscopic and microscopic analysis of all organs and tissues revealed no genotype-specific morphological differences. For appraisal of a putative motor-neuron pathology, brain, spinal cord and sciatic nerves were sectioned and stained by haematoxylin and eosin (H&E) and Klüver-Barrera; however, no abnormalities were detected. In particular, additional analysis of longitudinal sections of spinal cords derived from further homozygous N471D *Washc5* knock-in mice and their wild-type siblings (five of each genotype, aged 19 months) provided no evidence of a focal or generalised atrophy, demyelination or loss of neurons (Figure 2).

Because N471D *Washc5* knock-in mice were generated as a genetic model for human SPG8, the neurological tests are of particular interest. Notably, the assessment of basic neurological functions applying a modified SHIRPA protocol revealed that 17 of 32 (53%) of the heterozygous and 19 of 30 (63%) of the homozygous mice showed hind paw clenching when lifted by their tails as compared with 6 of 27 (22%) in the wild-type siblings (Figure 3A). All other SHIRPA parameters covering overall appearance, movement and reflexes were without any significant alteration. Normal results were also obtained for the additional tests of muscle function (grip strength), motor coordination (rotarod/beam ladder), balance (balance beam), auditory functions (ABR) and pain response (hotplate) in heterozygous as well as homozygous mice (Figure 2).

### Gait analysis of N471D *Washc5* knock-in mice reveal locomotor instability

The abnormal hind paw clenching of mutant mice, which was not a 'classical' clasping behaviour, as the fore paws' movements remained normal, prompted us to analyse the manner of walking using the DigiGait and CatWalk techniques that were performed at ages of 11 and 19 months, respectively. The DigiGait analysis, which was only performed using homozygous knock-in mice and wild-type siblings, resulted in various significantly aberrant values (Figure 3). In comparison with wild-type mice, mutant animals displayed increased forepaw swing (Figure 3B) and brake (Figure 3C) times that are temporal parameters of the portion of the stride in which the paw has no contact with the belt and the time between initial paw contact with the belt and the maximal paw contact during a stride, respectively. With regard to forepaw placement, the mutants ran with more outward turned paws, that is, with a positive value for the paw angular dimension (Figure 3D). The calculated forepaw values for the brake proportions of stride (Figure 3E) and of stance (Figure 3F), where stance refers to the portion of the stride in which the paw remains in contact with the belt, were increased in the homozygous animals. Moreover, the propel proportions, that is, the time fractions between the maximal paw to belt contact and the end of stride (Figure 3G) and stance (Figure 3H) were decreased. The CatWalk analysis, which was performed using both heterozygous and homozygous knock-in mice

as well as wild-type siblings, resulted in two further significantly affected parameters. Here, the homozygous animals displayed an increased hindpaw swing velocity (Figure 3I), which was also present in heterozygous mice but without reaching statistical significance. Moreover, homozygous mice displayed decreased body weight support on two diagonal paws during a stride and increased support on three paws (Figure 3J), most likely as a sign of locomotor instability. Taken together, these analyses depicted multiple gait abnormalities in homozygous mice, which solely express N471D mutated WASHC5.

### N471D mutated WASHC5 induced mild alterations in the global brain proteome

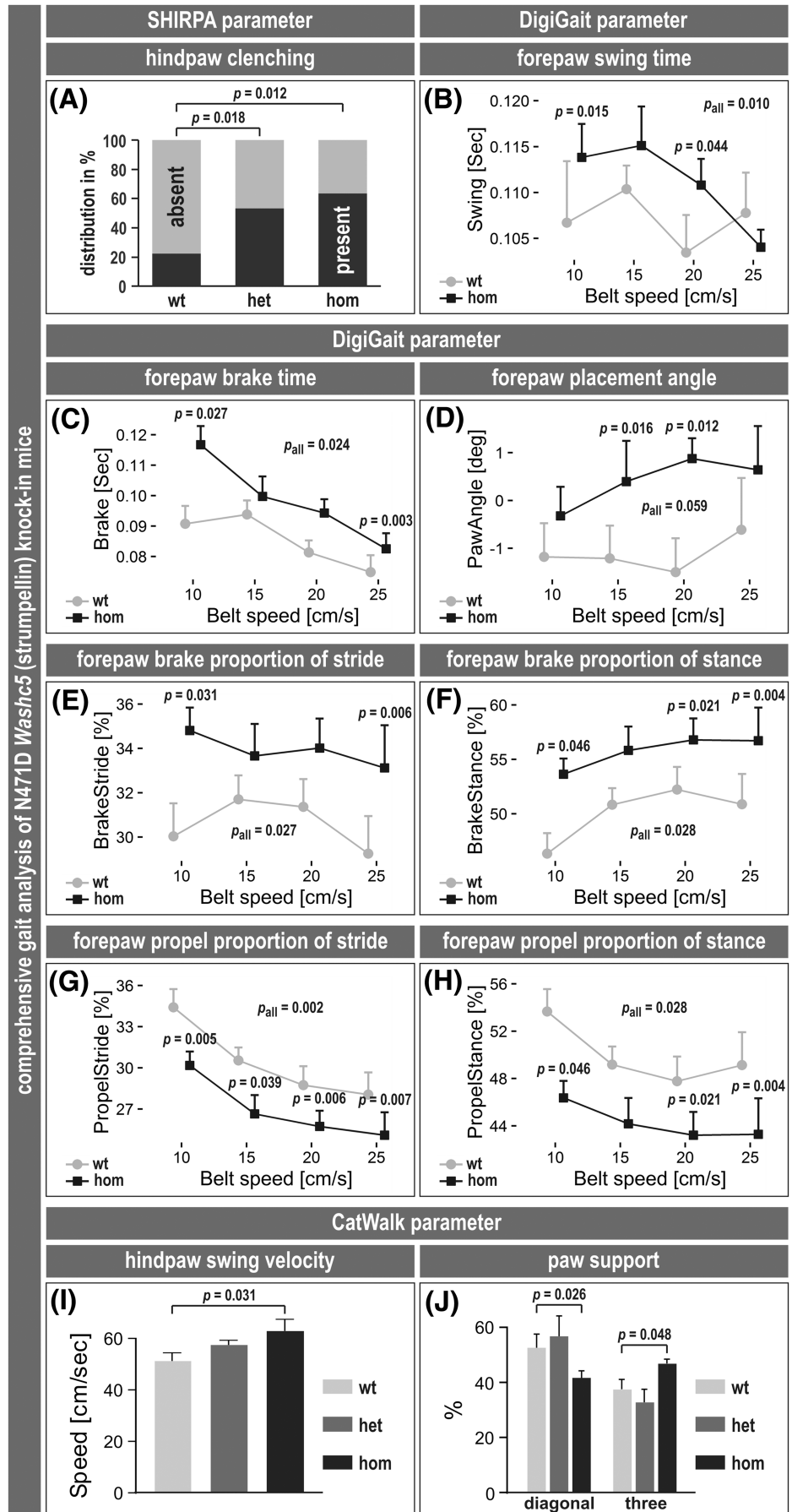
In order to gain insight into possible proteome changes induced by the presence of N471D mutated WASHC5, we performed quantitative mass spectrometry of total brain lysates from 2-year-old heterozygous ( $n = 5$ ) and homozygous ( $n = 6$ ) knock-in mice and wild-type littermates ( $n = 7$ ). In the three genotypes, a deep proteome of 8270 proteins was acquired at 1% FDR rate on both PSM and protein level with similar LFQ value distributions in all replicates (raw data and a method description have been deposited to the ProteomeXchange Consortium via the PRIDE partner repository [32] (<https://www.ebi.ac.uk/pride>) with the data set identifier PXD025315). Heat map and principal component (PCA) analyses demonstrated rather mild differences in the overall genotype-dependent protein expression profiles. In the heterozygous N471D *Washc5* knock-in condition, 217 proteins were significantly upregulated and 112 significantly downregulated with a fold-change  $\geq 2$  and a  $p$  value  $\leq 0.05$  as compared with the wild type. A comparison between homozygous and wild-type genotypes with the same statistical settings resulted in identification of 64 significantly upregulated and 30 significantly downregulated proteins (Figure 4A, blue dots). A subsequent analysis of the identified proteins with regard to gene ontology term enrichment, KEGG pathway enrichment, and protein interactions did not reveal additional aspects.

### The road not taken: Expression of N471D mutated WASHC5 did not alter abundance of the WASH, Arp2/3, retromer, retriever, and CCC complex constituents

WASHC5 is a component of the WASH complex, which acts as a nucleation promoting factor for the Arp2/3 complex-mediated actin polymerisation at the surface of endosomes [33–35]. A profile plot of the abundance of the individual protein constituents showed no change for either WASH complex Subunit 1 (WASHC1, WASH1), Subunit 2 (WASHC2, FAM21), Subunit 4 (WASHC4, SWIP, KIAA1033), Subunit 5 (WASHC5, KIAA0196, Strumpellin), CAPZA1, CAPZA2 or CAPZA3 (Figure 4B), while WASH complex Subunit 3 (WASHC3, CCD53) and CAPZA3 were not detected. A further profile plot showed no change for any Arp2/3 complex protein, that



**FIGURE 3** Gait analyses of N471D *Washc5* knock-in mice. Because heterozygous and homozygous mice showed increased rates of hindpaw clenching upon lifting at their tails (A), mice were examined for multiple gait-related parameters by the DigiGait (B–H, homozygous and wild-type mice) and CatWalk (I–J, mice of all three genotypes) systems. Swing time (B), portion of the stride in which the paw has no contact with the belt. Brake time (C), time between initial paw contact with the belt and the maximal paw contact during a stride. Placement angle (D), angle that the paws make with the long axis of the direction of motion of an animal. Brake proportion of stride (E), portion of the stride between initial paw contact with the belt and the maximal paw contact during a stride. Brake proportion of stance (F), portion of the stance between initial paw contact with the belt and the maximal paw contact. Stance refers to the portion of the stride in which the paw remains in contact with the belt. Propel proportion of stride (G), time fraction between the maximal paw to belt contact and the end of stride. Propel proportion of stance (H), time fraction between the maximal paw to belt contact and the end of stance. Swing velocity (I), velocity of the stride portion in which the paw has no contact with the glass plate. Paw support (J), time fractions of a stride with body weight support on two diagonal paws (left columns) and three paws (right columns) having contact with the glass plate



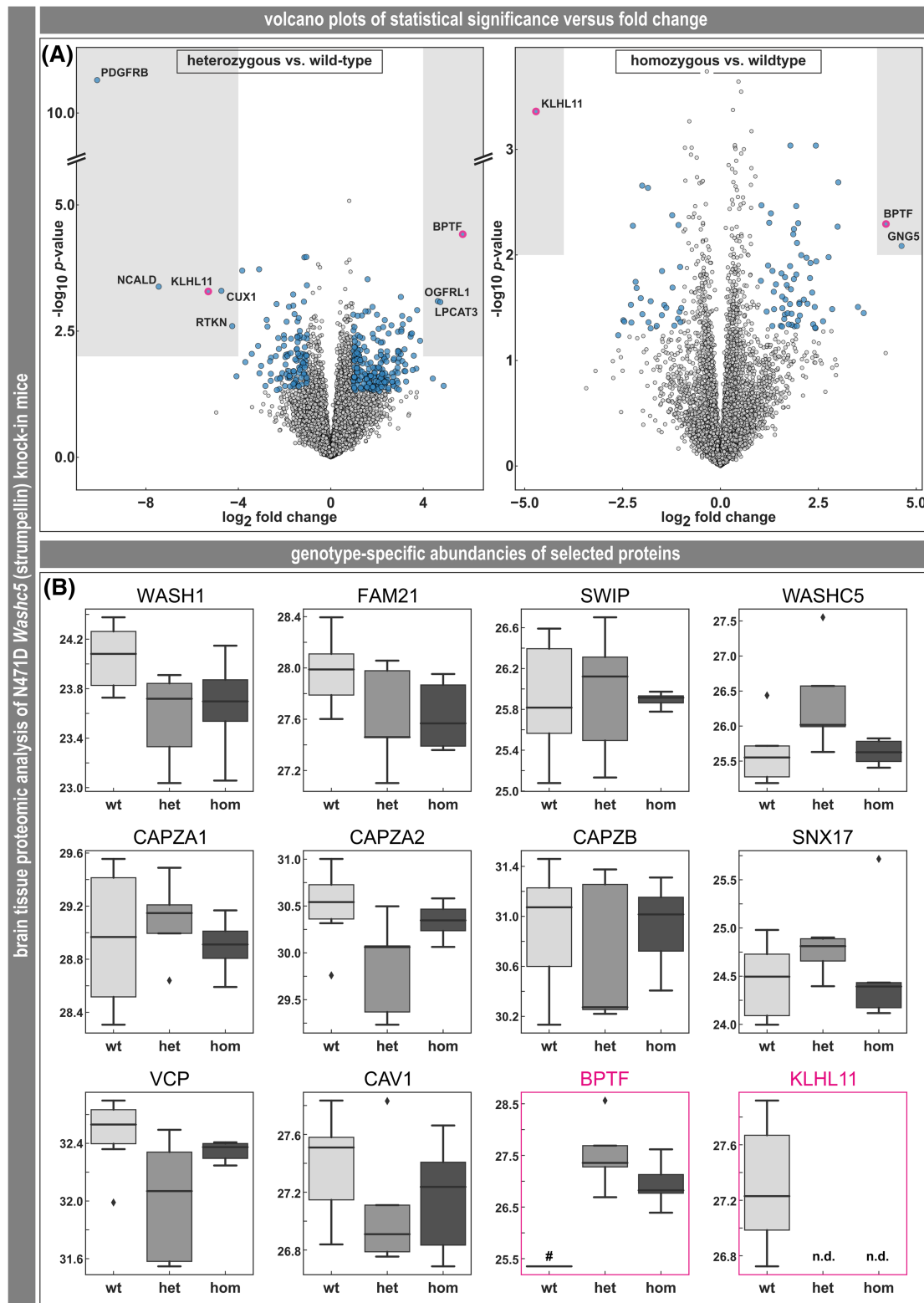


**FIGURE 4** Proteomic analysis of brain tissue derived from N471D *Washc5* knock-in mice. Volcano plots comparing protein levels of heterozygous versus wild-type (A, left plot) as well as homozygous versus wild-type genotypes (A, right plot). x-axis,  $\log_2$ -transformed mean fold change; y-axis,  $-\log_{10}$  transformed  $p$  value. Note the consistent upregulation of BPTF and downregulation of KLHL11 in both genotypes (magenta circles). Blue dots indicate significantly regulated proteins with a fold-change  $\geq 2$  and a  $p$  value  $\leq 0.05$ . Grey rectangular areas highlight most significant changes with a fold change  $\geq 16$  and a  $p$  value  $\leq 0.01$ . (B) Box plot illustrations of the abundancies of selected protein candidates (please refer to the Section 3). Significant changes in the abundancies were only detected for BPTF and KLHL11 (magenta frame). y-axis,  $\log_2$ -transformed label-free quantitation (LFQ) values. Small diamonds, individual outliers; hash, detected in only one biological replicate; n.d., not detected

is, ARP2/ACTR2, ARP3/ACTR3, p41/ARPC1A, p41/ARPC1B, p34/ARPC2, p21/ARPC3, p20/ARPC4, p16/ARPC5 and ARPC5L. Because there are components with a dual role in the WASH and retromer complexes as well as the retromer and retriever complexes, respectively, and there is a functional complementarity of the WASH, retromer, retriever, and CCC complexes in endosomal protein sorting and recycling [33, 34, 36], we also generated profile plots of these complexes and the CCC complex interacting protein SNX17. The abundancies of all proteins of the retromer complex (WASHC1, WASHC2, VPS26A, VPS26B, VPS29, VPS35, SNX1, SNX2, SNX5, SNX6) were unchanged in hetero- and homozygous animals. The same holds true for the retriever complex (DSCR3 [VPS26], C16ORF62 homologue, VPS29) with exception for VPS35 that was not detected in any genotype. Finally, addressing the CCC complex and SNX17, the abundancies of CCDC93, CCDC22, and SNX17 did not differ between knock-in and wild-type mice (Figure 4B), while COMMD1 could not be detected.

### Expression of N471D mutated WASHC5 did not induce changes in the abundancies of proven and putative binding partners

WASHC5 is a multi-functional protein with a series of established binding partners in the above protein complexes (see UniProtKB entries Q12768 and Q8C2E7). In addition, we demonstrated a direct interaction between WASHC5 and the AAA ATPase VCP (TERA) [17] that is implicated in the pathogenesis of various neurodegenerative diseases [37]. However, no change in VCP abundancy between the three genotypes could be detected (Figure 4B). Furthermore, an interaction of WASHC5 with CAV1 and dependence of CAV1 levels from the integrity of the WASH complex was reported [38]. The expression of N471D mutated WASHC5 did not rescue reduced CAV1 levels in cultured retina epithelial cells with endogenous WASHC5 depletion [38]. Our proteomics analysis, however, did not reveal a change in the abundancy of CAV1 (Figure 4B).

In addition to its well-established binding partners, results from our previous immunoprecipitation studies yielded several putative novel WASHC5 interacting proteins. Using lysates of doubly transfected HEK293 cells over-expressing VCP-GFP and mCherry-WASHC5 fusion proteins in conjunction with anti-RFP mAb coated beads, we co-immunoprecipitated HSP90B1, ENO1, ACTB, CKB, ALDOA, GAPDH, LDHB and YWHAE. A profile plot of these proteins showed no significant changes in the abundance of these proteins. In another experiment, we performed a series of co-immunoprecipitations using three different rabbit polyclonal antibodies directed against WASHC5 (str\_2\_7110, [18]), SWIP (swip\_7\_7762, [18]), and VCP (p97\_9\_6574, [39]) in conjunction with lysates from AX2 wild-type *Dictyostelium discoideum* cells. The intersection set of the three immunoprecipitates comprised common protein candidates of which DDB\_G0276417/PDHB (Dicty base ID/murine ortholog), DDB\_G0275029/DLST, DDB\_G0277847/DLAT, DDB\_G0288127/OGDH, DDB\_G0269144/

HSP70, DDB\_G0293298/HSPA9 and DDB\_G0292994/PDHA1 showed no changed abundancies, whereas DDB\_G0291127/MVP was not detected in the present analysis. Finally, a total of 116 putative Washc5 binding partners was identified by co-immunoprecipitation experiments using washc5 knock-out *Dictyostelium discoideum* cells either stably expressing wild-type Washc5-GFP or N471D mutated Washc5-GFP fusion proteins as well as AX2 wild-type *Dictyostelium discoideum* cells stably expressing GFP for control (see table S1 in the supporting information of Song et al. [18]). A subset of 43 protein candidates displayed either significantly reduced or even no binding to N471D mutated Washc5. Murine orthologs could be assigned to 59 of the 73 putative Washc5 interactors and to 41 of the 43 candidates without N471D Washc5 binding; however, for none of these proteins significant changes in their abundancies were detected.

### Expression of N471D mutated WASHC5 induced consistent upregulation of BPTF and downregulation of KLHL11 in brain tissue of heterozygous and homozygous knock-in mice

While the hypothesis-driven analysis of specific proteins described above did not result in identification of protein sets with altered expression levels, the comparison of the proteomic data sets derived from heterozygous N471D *Washc5* knock-in mice and wild-type littermate brains demonstrated BPTF, OGFRL1 and LPCAT3 as most significantly ( $p \leq 0.01$ , shown as negative decadic logarithm of the  $p$  value) and markedly (fold change  $\geq 16$ , shown as binary logarithm of the fold change) upregulated, and PDGFRB, NCALD, KLHL11, CUX1 and RTKN as most significantly and markedly downregulated proteins. In the analogous setting for homozygous N471D *Washc5* mice, BPTF and GNG5 were found to be upregulated, and KLHL11 was downregulated (Figure 4A, grey rectangular areas). Notably, the comparison of all three genotypes yielded a common set comprising two distinct proteins, namely, BPTF (NURF subunit BPTF or Nucleosome-remodelling factor subunit bromodomain and PHD finger-containing transcription factor) and KLHL11 (Kelch-like protein 11) (Figure 4A, magenta circles). Whereas the former was consistently upregulated in heterozygous and homozygous conditions, the latter showed a marked downregulation (Figure 4B). However, further profile plots of NURF complex components and several known BPTF-related single interacting proteins (see BPTF UniProtKB entries Q12830 and Q6P9L3) showed no change for any of the other NURF constituents SMARCA1, RBBP4 and RBBP7, as well as the BPTF-interacting proteins MAZ, H32 and H4; the BPTF interaction partners KEAP1, SMCA1 were not detected. Likewise, profile plots of the KLHL11-related interacting proteins UBQLN2 and CUL3 (see KLHL11 UniProtKB entries Q9NVR0 and Q8CE33) revealed no change, while KLHL11 binding partners IHO1 and PO6F2 were not detected. Taken together, this bioinformatic analysis eventually resulted in the identification of two distinct proteins that are of high interest because of their relation to neurodegeneration and protein quality control.

## DISCUSSION

In humans, the heterozygous expression of N471D mutated WASHC5 leads to a progressive upper motor-neuron degeneration leading to spasticity of the lower limbs usually beginning between the second and sixth decade of life [1]. In a subset of patients, additional upper limb ataxia [40], muscle wasting of the lower limbs, urinary bladder-control problems and sensory axonal neuropathy [2, 41, 42] have been reported. In the corresponding heterozygous N471D *Washc5* knock-in mice, our phenotypic analysis only showed an increased rate of hindpaw clenching, mildly increased levels of alkaline phosphatase and of potassium, elevated white blood cell counts and lowered lactate levels. Though the hindpaw clenching may be interpreted as a sign of motor dysfunction, the clinical phenotype and the neuropathological evaluation of central nervous tissue did not provide evidence that the heterozygous expression of N471D mutated WASHC5 resulted in an upper motor-neuron phenotype equivalent to the human situation. However, similar changes, but in a more accentuated fashion, were present in homozygous animals, which furthermore displayed elevated haemoglobin concentrations, thinner eye lenses (limited to male mice) and decreased acoustic startle reactivity. Homozygous animals solely expressing N471D mutated WASHC5 also showed increased left ventricle diameter, mass and stroke volume as well as multiple aberrant gait parameters indicating a mild locomotor instability. Although these findings clearly suggest that N471D mutated WASHC5 interferes with structural or functional integrity of cardiac and nervous tissue, the observed murine phenotypes neither mirror the clinical picture of hereditary spastic paraplegia 8 nor that of Ritscher-Schinzel syndrome 1. In keeping with a previous study, our attempts to breed homozygous *Washc5* knock-out mice failed, thus supporting the notion that the absence of WASHC5 is lethal [13]. Notably, and in contrast to the aforementioned study reporting markedly reduced protein levels, our heterozygous *Washc5* knock-out animals showed WASHC5 levels identical to those in wild-type littermates. Because heterozygous *Washc5* knock-out animals showed no phenotypic abnormalities [13], there is no evidence that inactivation of one *Washc5* allele, irrespective of the effects on the molecular level, leads to a disease phenotype related to either hereditary spastic paraplegia 8 or Ritscher-Schinzel syndrome 1.

WASHC5 contains a central domain of five spectrin-like repeats, which may serve as a platform for protein-protein interactions [43], for example, in the WASH complex [44]. To further address the effects of the expression of the N471D mutation, which is located in the third spectrin-like repeat, we performed a deep proteomic analysis of central nervous tissue derived from aged heterozygous and homozygous N471D *Washc5* knock-in mice and wild-type littermates. Notably, neither any of the WASH complex constituents nor of the related Arp2/3, retromer, retriever and CCC complexes showed significant changes in their abundancies that were consistent in both genotypes. Moreover, no relevant changes could be detected analysing VCP [17], CAV1 [38], and a large number of putative WASHC5 interaction partners as described above. Thus, the present quantitative proteomic analysis of murine brain tissue derived from heterozygous

and homozygous N471D *Washc5* knock-in mice depicted a different pattern than the previously reported changes induced by reduced or absent WASH complex subunit 5 expression in *Dictyostelium discoideum* [18, 45], mammalian cells [46] and murine tissue [13]. In those studies, downregulation or knock-out of WASH complex subunit 5 resulted in decreased amounts of at least one other WASH complex subunit. Notably, the exclusive presence of N471D mutated WASH complex subunit 5 in *Dictyostelium discoideum* [18] and in brain tissue of N471D *Washc5* knock-in mice (this work) did not alter the abundancies of the other WASH complex subunits. In contrast to a lack of WASHC5, this observation argues against a N471D mutated WASHC5-induced destabilisation of the WASH complex with consecutive degradation of its individual components.

The proteomic analysis of central nervous tissue reported here resulted in the identification of two proteins of interest in both the heterozygous and homozygous conditions, namely BPTF (NURF subunit BPTF or Nucleosome-remodelling factor subunit bromodomain and PHD finger-containing transcription factor) and KLHL11 (Kelch-like protein 11), which were consistently upregulated and downregulated, respectively. With regard to SPG8 and RTSC1, it is noteworthy that heterozygous *BPTF* (synonyms: *FAC1*, *FALZ*) mutations have been described to cause NEDDFL, a neurodevelopmental disorder with dysmorphic facies and distal limb anomalies, clinically presenting with developmental delay, intellectual disability, speech delay, postnatal microcephaly, seizures, motor delay, hypotonia, scoliosis and dysmorphic face and limb features as well as ophthalmologic complications [47, 48]. BPTF, which primarily localises to the cell body and nuclei of spinal cord motor neurons during development, has been described to be upregulated in surviving spinal cord motor neurons in patients suffering from amyotrophic lateral sclerosis [49]. Thus, BPTF upregulation seems to be a shared feature between SPG8 and ALS. In contrast, the second protein of interest, KLHL11, showed a consistent downregulation. KLHL11 is a component of a cullin-RING-based BCR (BTB-CUL3-RBX1) E3 ubiquitin-protein ligase complex [50] mediating ubiquitination of target proteins [51]. Although the presence of antibodies directed against KLHL11 has been identified as biomarker of a paraneoplastic neurological syndrome [52, 53], the function of KLHL11 remains to be elucidated. In the context of SPG8 it is tempting to speculate that downregulation of KLHL11 may contribute to the disease progression, owing to its putative function in protein quality control.

Previous studies controversially discussed the issue of the *WASHC5* mutation-related disease mechanism either favouring (i) a loss-of-function in the recessively inherited Ritscher-Schinzel syndrome 1 [3] or (ii) a haploinsufficiency based gene dosage, gene expression or protein activity effect, (iii) a dominant-negative effect or (iv) gain-of-function by increased protein activity or toxic gain-of-function [54] in the dominantly inherited spastic paraplegia 8 [1, 15, 17, 38, 46, 55, 56]. Though our proteomic analysis of heterozygous and homozygous N471D *Washc5* knock-in mice showed no rectified changes in the abundancies of either WASH complex subunits nor related complexes and WASHC5 binding partners, the phenotypic analysis of several alterations that were more accentuated in homozygous than in heterozygous animals indicated a gene dosage

effect of the N471D mutation as previously suggested [41]. However, the present results from the combined phenotypic and proteomic analyses do not allow a clear attribution of the N471D mutation-induced pathophysiology to one of the above-mentioned mutation-related disease mechanisms. To resolve this issue, additional insights into the altered function of mutated WASHC5 at the molecular level are required.

## ACKNOWLEDGEMENTS

I. W. was funded by the Deutsche Forschungsgemeinschaft (DFG) (FOR5046/P5) and by the Cardio Pulmonary Institute (CPI) of the DFG (EXC2026). MHdA was funded by the German Federal Ministry of Education and Research (Infrafrontier grant 01KX1012) and the German Center for Diabetes Research (DZD).

## CONFLICT OF INTEREST

The authors declare that they have no conflict of interest.

## AUTHOR CONTRIBUTIONS

C. S. C. and R. S. jointly conceived the study, reviewed all data, prepared the final figures and wrote the manuscript. C. S. C., L. W., F. C., I. W., L. B., The German Mouse Clinic Consortium (see Appendix A), V. G. D., H. F., M. H. d. A., and L. E. designed and carried out experiments and analysed data. C. B. carried out experiments and analysed data. A. S., R. C., A. H., B. E., K. M., M. K., S. v. H. and R. S. designed experiments and analysed data. All authors read and approved the final version of manuscript text and figures.

## ETHICS STATEMENT

All procedures involving mice were approved by the responsible authorities as described in the Section 2.

## PEER REVIEW

The peer review history for this article is available at <https://publons.com/publon/10.1111/nan.12750>.

## DATA AVAILABILITY STATEMENT

The data that support the findings of this study are openly available as described in the Section 3.

## ORCID

Christoph S. Clemen  <https://orcid.org/0000-0002-1291-4219>

Lilli Winter  <https://orcid.org/0000-0002-6368-1160>

Rolf Schröder  <https://orcid.org/0000-0002-2772-2615>

## REFERENCES

1. Valdmanis PN, Meijer IA, Reynolds A, et al. Mutations in the KIAA0196 gene at the SPG8 locus cause hereditary spastic paraplegia. *Am J Hum Genet.* 2007;80(1):152-161.
2. Ginanneschi F, D'Amore A, Barghigiani M, et al. SPG8 mutations in Italian families: clinical data and literature review. *Neurological Sciences: Official Journal of the Italian Neurological Society and of the Italian Society of Clinical Neurophysiology.* 2020;41(3):699-703.
3. Elliott AM, Simard LR, Coghlan G, et al. A novel mutation in KIAA0196: identification of a gene involved in Ritscher-Schinzel/3C syndrome in a First Nations cohort. *J Med Genet.* 2013;50(12):819-822.
4. Elliott AM, Chudley A. Ritscher-Schinzel syndrome. In: Adam MP, Ardinger HH, Pagon RA, et al., editors. *GeneReviews*<sup>®</sup>. Seattle WA, 2020.
5. Lo Giudice T, Lombardi F, Santorelli FM, Kawarai T, Orlacchio A. Hereditary spastic paraplegia: clinical-genetic characteristics and evolving molecular mechanisms. *Exp Neurol.* 2014;261:518-539.
6. Murala S, Nagarajan E, Bollu PC. Hereditary spastic paraplegia. *Neurological Sciences: Official Journal of the Italian Neurological Society and of the Italian Society of Clinical Neurophysiology.* 2021;42(3):883-894.
7. Blackstone C. Hereditary spastic paraplegia. *Handb Clin Neurol.* 2018;148:633-652.
8. Leonardi ML, Pai GS, Wilkes B, Lebel RR. Ritscher-Schinzel cranio-cerebello-cardiac (3C) syndrome: report of four new cases and review. *Am J Med Genet.* 2001;102(3):237-242.
9. Jahic A, Kreuz F, Zacher P, et al. A novel strumpellin mutation and potential pitfalls in the molecular diagnosis of hereditary spastic paraplegia type SPG8. *J Neurol Sci.* 2014;347(1-2):372-374.
10. Bogucki P, Sobczynska-Tomaszewska A. First patient with hereditary spastic paraplegia type 8 in Poland. *Clin Case Rep.* 2017;5(9):1468-1470.
11. Aberle H, Bauer A, Stappert J, Kispert A, Kemler R. beta-catenin is a target for the ubiquitin-proteasome pathway. *EMBO J.* 1997;16(13):3797-3804.
12. Schüle R, Wiethoff S, Martus P, et al. Hereditary spastic paraplegia: clinico-genetic lessons from 608 patients. *Ann Neurol.* 2016;79(4):646-658.
13. Jahic A, Khundadze M, Jaenisch N, et al. The spectrum of KIAA0196 variants, and characterization of a murine knockout: implications for the mutational mechanism in hereditary spastic paraplegia type SPG8. *Orphanet J Rare Dis.* 2015;10(1):147.
14. Elert-Dobkowska E, Stepniak I, Krysa W, et al. Next-generation sequencing study reveals the broader variant spectrum of hereditary spastic paraplegia and related phenotypes. *Neurogenetics.* 2019;20(1):27-38.
15. Ma L, Shi Y, Chen Z, Li S, Qin W, Zhang J. A novel KIAA0196 mutation in a Chinese patient with spastic paraplegia 8: a case report. *Medicine (Baltimore).* 2018;97(20):e10760.
16. Pehrson C, Hertz JM, Wirenfeldt M, Stenager E, Wermuth L, Winther Kristensen B. Hereditary spastic paraplegia type 8: neuropathological findings. *Brain Pathol.* 2018;28(2):292-294.
17. Clemen CS, Tangavelou K, Strucksberg KH, et al. Strumpellin is a novel valosin-containing protein binding partner linking hereditary spastic paraplegia to protein aggregation diseases. *Brain.* 2010;133(10):2920-2941.
18. Song L, Rijal R, Karow M, et al. Expression of N471D strumpellin leads to defects in the endolysosomal system. *Dis Model Mech.* 2018;11.
19. Gailus-Durner V, Fuchs H, Becker L, et al. Introducing the German Mouse Clinic: open access platform for standardized phenotyping. *Nat Methods.* 2005;2(6):403-404.
20. Fuchs H, Gailus-Durner V, Adler T, et al. The German Mouse Clinic: a platform for systemic phenotype analysis of mouse models. *Curr Pharm Biotechnol.* 2009;10(2):236-243.
21. Fuchs H, Gailus-Durner V, Neschen S, et al. Innovations in phenotyping of mouse models in the German Mouse Clinic. *Mamm Genome.* 2012;23(9-10):611-622.
22. Fuchs H, Gailus-Durner V, Adler T, et al. Mouse phenotyping. *Methods.* 2011;53(2):120-135.
23. Minakaki G, Caneva F, Chevessier F, et al. Treadmill exercise intervention improves gait and postural control in alpha-synuclein mouse models without inducing cerebral autophagy. *Behav Brain Res.* 2019;363:199-215.

24. Timotius IK, Canneva F, Minakaki G, et al. Dynamic footprint based locomotion sway assessment in alpha-synucleinopathic mice using Fast Fourier transform and low pass filter. *J Neurosci Methods*. 2018; 296:1-11.
25. Timotius IK, Mocerri S, Plank AC, et al. Silhouette-length-scaled gait parameters for motor functional analysis in mice and rats. *eNeuro*. 2019;6(6):ENEURO.0100-ENEU19.2019.
26. Timotius IK, Canneva F, Minakaki G, et al. Systematic data analysis and data mining in CatWalk gait analysis by heat mapping exemplified in rodent models for neurodegenerative diseases. *J Neurosci Methods*. 2019;326:108367.
27. Winter L, Unger A, Berwanger C, et al. Imbalances in protein homeostasis caused by mutant desmin. *Neuropathol Appl Neurobiol*. 2019; 45(5):476-494.
28. Lowry OH, Rosebrough NJ, Farr AL, Randall RJ. Protein measurement with the Folin phenol reagent. *J Biol Chem*. 1951;193(1): 265-275.
29. Wiśniewski JR, Zougman A, Nagaraj N, Mann M. Universal sample preparation method for proteome analysis. *Nat Methods*. 2009;6(5): 359-362.
30. Rappsilber J, Mann M, Ishihama Y. Protocol for micro-purification, enrichment, pre-fractionation and storage of peptides for proteomics using StageTips. *Nat Protoc*. 2007;2(8):1896-1906.
31. Nolte H, MacVicar TD, Tellkamp F, et al. Instant Clue: a software suite for interactive data visualization and analysis. *Sci Rep*. 2018; 8(1):12648.
32. Perez-Riverol Y, Csordas A, Bai J, et al. The PRIDE database and related tools and resources in 2019: improving support for quantification data. *Nucleic Acids Res*. 2019;47(D1):D442-D450.
33. Simonetti B, Cullen PJ. Actin-dependent endosomal receptor recycling. *Curr Opin Cell Biol*. 2019;56:22-33.
34. Seaman MN, Gautreau A, Billadeau DD. Retromer-mediated endosomal protein sorting: all WASHed up! *Trends Cell Biol*. 2013; 23(11):522-528.
35. Rottner K, Hänisch J, Campellone KG. WASH, WHAMM and JMY: regulation of Arp2/3 complex and beyond. *Trends Cell Biol*. 2010; 20(11):650-661.
36. Chen KE, Healy MD, Collins BM. Towards a molecular understanding of endosomal trafficking by Retromer and Retriever. *Traffic*. 2019; 20(7):465-478.
37. Evangelista T, Weihi CC, Kimonis V, et al. 215th ENMC International Workshop VCP-related multi-system proteinopathy (IBMPFD) 13-15 November 2015, Heemskerk, The Netherlands. *Neuromuscul Disord*. 2016;26(8):535-547.
38. Lee S, Park H, Zhu PP, Jung SY, Blackstone C, Chang J. Hereditary spastic paraplegia SPG8 mutations impair CAV1-dependent, integrin-mediated cell adhesion. *Sci Signal*. 2020;13(613):eaau7500.
39. Arhzaouy K, Strucksberg KH, Tung SM, et al. Heteromeric p97/p97R155C complexes induce dominant negative changes in wild-type and autophagy 9-deficient Dictyostelium strains. *PLoS ONE*. 2012;7(10):e46879.
40. Ichinose Y, Koh K, Fukumoto M, et al. Exome sequencing reveals a novel missense mutation in the KIAA0196 gene in a Japanese patient with SPG8. *Clin Neurol Neurosurg*. 2016;144:36-38.
41. Meijer IA, Valdmanis PN, Rouleau GA. In: Adam MP, Ardinger HH, Pagon RA, et al., eds. *Spastic Paraplegia* 8. Seattle WA: GeneReviews®; 2008 updated 2020.
42. Bettencourt C, Morris HR, Singleton AB, Hardy J, Houlden H. Exome sequencing expands the mutational spectrum of SPG8 in a family with spasticity responsive to L-DOPA treatment. *J Neurol*. 2013; 260(9):2414-2416.
43. Djinovic-Carugo K, Gautel M, Ylänen J, Young P. The spectrin repeat: a structural platform for cytoskeletal protein assemblies. *FEBS Lett*. 2002;513(1):119-123.
44. Derivery E, Sousa C, Gautier JJ, Lombard B, Loew D, Gautreau A. The Arp2/3 activator WASH controls the fission of endosomes through a large multiprotein complex. *Dev Cell*. 2009;17(5):712-723.
45. Park L, Thomason PA, Zech T, et al. Cyclical action of the WASH complex: FAM21 and capping protein drive WASH recycling, not initial recruitment. *Dev Cell*. 2013;24(2):169-181.
46. Jia D, Gomez TS, Metlagel Z, et al. WASH and WAVE actin regulators of the Wiskott-Aldrich syndrome protein (WASP) family are controlled by analogous structurally related complexes. *Proc Natl Acad Sci U S A*. 2010;107(23):10442-10447.
47. Stankiewicz P, Khan TN, Szafranski P, et al. Haploinsufficiency of the chromatin remodeler BPTF causes syndromic developmental and speech delay, postnatal microcephaly, and dysmorphic features. *Am J Hum Genet*. 2017;101(4):503-515.
48. Grinton KE, Hurst ACE, Bowling KM, et al. Phenotypic expansion of the BPTF-related neurodevelopmental disorder with dysmorphic facies and distal limb anomalies. *Am J Med Genet A*. 2021;185(5): 1366-1378.
49. Mu X, Springer JE, Bowser R. FAC1 expression and localization in motor neurons of developing, adult, and amyotrophic lateral sclerosis spinal cord. *Exp Neurol*. 1997;146(1):17-24.
50. Canning P, Cooper CD, Krojer T, et al. Structural basis for Cul3 protein assembly with the BTB-Kelch family of E3 ubiquitin ligases. *J Biol Chem*. 2013;288(11):7803-7814.
51. Dhanoa BS, Cogliati T, Satish AG, Bruford EA, Friedman JS. Update on the Kelch-like (KLHL) gene family. *Hum Genomics*. 2013;7(1):13.
52. Dubey D, Wilson MR, Clarkson B, et al. Expanded clinical phenotype, oncological associations, and immunopathologic insights of paraneoplastic Kelch-like Protein-11 encephalitis. *JAMA Neurol*. 2020; 77(11):1420-1429.
53. Maudes E, Landa J, Munoz-Lopetegui A, et al. Clinical significance of Kelch-like protein 11 antibodies. *Neurology(R) Neuroimmunology & Neuroinflammation*. 2020;7.
54. Wilkie AO. The molecular basis of genetic dominance. *J Med Genet*. 1994;31(2):89-98.
55. Freeman C, Seaman MNJ, Reid E. The hereditary spastic paraplegia protein strumpellin: Characterisation in neurons and of the effect of disease mutations on WASH complex assembly and function. *Biochim Biophys Acta*. 2013;1832(1):160-173.
56. Harbour ME, Breusegem SY, Antrobus R, et al. The cargo-selective retromer complex is a recruiting hub for protein complexes that regulate endosomal tubule dynamics. *J Cell Sci*. 2010;123(21): 3703-3717.

**How to cite this article:** Clemen CS, Schmidt A, Winter L, et al. N471D WASH complex subunit strumpellin knock-in mice display mild motor and cardiac abnormalities and BPTF and KLHL11 dysregulation in brain tissue. *Neuropathol Appl Neurobiol*. 2022;48(1):e12750. <https://doi.org/10.1111/nan.12750>

## APPENDIX

German Mouse Clinic, Institute of Experimental Genetics, Helmholtz Zentrum München, German Research Center for Environmental Health, 85764 Neuherberg, Germany:

Antonio Aguilar-Pimentel<sup>1</sup>, Carsten Schmidt-Weber<sup>2</sup>, Irina Treise<sup>1,3</sup>, Dirk H. Busch<sup>3</sup>, Nadine Spielmann<sup>1</sup>, Oana V. Amarie<sup>1</sup>, Jan Rozman<sup>1,4</sup>, Lillian Garrett<sup>1,5</sup>, Sabine M. Hölter<sup>1,5,6</sup>, Wolfgang

Wurst<sup>5,6,7</sup>, Julia Calzada-Wack<sup>1</sup>, Patricia da Silva-Buttkus<sup>1</sup>, Birgit Rathkolb<sup>1,4,8</sup>, Eckhard Wolf<sup>8</sup>, Manuela A. Östreichner<sup>1</sup>, Holger Maier<sup>1</sup>, Stefanie Leuchtenberger<sup>1</sup>, Claudia Stoeger<sup>1</sup>

<sup>1</sup> Institute of Experimental Genetics, German Mouse Clinic, Helmholtz Zentrum München, German Research Center for Environmental Health, 85764 Neuherberg, Germany

<sup>2</sup> Center of Allergy & Environment (ZAUM), Technische Universität München, and Helmholtz Zentrum München, 85764 Neuherberg, Germany

<sup>3</sup> Institute for Medical Microbiology, Immunology and Hygiene, Technical University of Munich, 81675 Munich, Germany

<sup>4</sup> Member of German Center for Diabetes Research (DZD), 85764 Neuherberg, Germany

<sup>5</sup> Institute of Developmental Genetics, Helmholtz Zentrum München, German Research Center for Environmental Health, 85764 Neuherberg, Germany

<sup>6</sup> Chair of Developmental Genetics, TUM School of Life Sciences (SoLS), Technische Universität München, 85354 Freising-Weihenstephan, Germany

<sup>7</sup> Deutsches Institut für Neurodegenerative Erkrankungen (DZNE) Site Munich, 80336 Munich, Germany

<sup>8</sup> Ludwig-Maximilians-Universität München, Gene Center, Institute of Molecular Animal Breeding and Biotechnology, 81377 Munich, Germany